Vilniaus university
Faculty of Physics
Laser reasearch centre

Matas Mitrikas

EXTENSION OF WORKING DISTANCE OF HIGH NUMERICAL APERTURE OBJECTIVE FOR MESOSCALE OBJECTS FABRICATION

FINAL THESIS OF BACHELOR STUDIES

Light engineering program

Student	Matas Mitrikas
Superwisor	doct. Agnė Butkutė
Institute direktor	prof. Aidas Matijošius

Vilnius 2023

Contents

Introduction

Laser have significantly influenced various fields of study and industry. Ever since the first publication of a ruby laser by T. H. Maiman[1], advancements have continued. Refinement of different gain mediums as well as the development of ultra-short laser pulses had paved a way to create a contact-free tool, possessing high precision and capable of micro and macro machining. Due to these properties lasers have been implemented for a variety of applications, such as: communication[2], [3], industrial fabrication[4], biology[5], medicine[6]–[8] and microtechnologies[9]. In the latter fields the introduction of lasers has greatly increased their capabilities. Implementation of two-photon polymerization (2PP) created a way to produce complex 3D structures, with nm size features[10]. However, in conventional 2PP process, the structure height is limited by the working distance of the microscope objective used in laser focusing. Additional configurations have been proposed in order to widen objective working field. A simple, cheap and universaly viable solution has been proposed by K. Obata et. Al called WOW-2PP[11]. This configuration allows the creation supreme mesoscale object that posses sub-wavelength sized features by extending the working distance of high numerical aperture (NA) objectives.

The main goal of this bachelor's thesis was to produce a method for creating large-scale structures with micrometre sized features. Course work tasks were:

- Create a cheap and simple device to increase the working distance of a 63x1.4 objective;
- Test the maximum possible height of polymeric structure created with this technique;
- Fabricate high resolution large-scale structures using ORMOCOMP.

1. Literature review:

1.1 Light interaction with matter

It is generally accepted, that materials can either reflect, absorb, transmit or scatter the incoming light. Having said this, as this work is mainly concentrated on the effects of absorption, working principles of other interactions processes will be excluded.

Simply put, absorption is a process, where the incoming light is converted into a different form of energy. This phenomenon occurs when the incoming photon energy is higher than the materials bandgap. A single photon is then absorbed by a single electron, thus the transition from the conduction to the valance band takes place. After absorbing a photon, an excited electron can release the acquired energy in many ways, like fluorescence, phosphorescence, or Auger recombination just to name a few[12]. Absorption, when induced with laser radiation, depends on a lot of parameters such as: laser wavelength (λ) (1.1), intensity (I) (1.2), material absorption coefficient (α) (1.3), etc. A wide range of materials are thus susceptible to this phenomenon, which includes metals, insulators, dielectrics and semiconductors.

$$\lambda = \frac{v}{f} \tag{1.1}$$

$$I(r) = I_0 exp\left(-\frac{r^2}{\omega_0^2}\right) \tag{1.2}$$

$$\alpha = \frac{4\pi k}{\lambda} \tag{1.3}$$

In the field of laser material processing selective exposure of sufficient amount of light is used to create desired changes in the selected medium. During early developments, energy inside the material was introduced through linear absorption by inducing photons of the same or higher energies than the substances band gap. As the photon energy is dependent on the emission wavelength ($E_p = hc/\lambda$), different materials require discrete wavelengths to be processed. For example, in the field of metal cutting CO_2 were widespread[13], while processing of polymers was mainly done with excimer lasers[14]. However, with the introduction of Q-switched lasers as well as the implementation of mode synchronization drastically shortened laser pulse durations. This reduction in time drastically increased the peak power of laser systems (1.4).

$$P_p = \frac{P}{\pi\omega_0^2} \tag{1.4}$$

Pairing high peak power laser systems with focusing optics a sharp increase in light intensity at the focal volume can be achieved. It can be expressed as:

$$I = \frac{2P}{\pi\omega_0^2} \tag{1.5}$$

here ω_0 is the laser spot radius.

During this work transparent dielectric was processed. These substances have low absorbance for the lasing wavelength (780 nm)[15], however, in response to high intensities, this material undergoes nonlinear phenomena. Recently developments of femtosecond laser pulses have made it possible to reach intensities that are approximately equal to E^2. If E exceeds a value of 10^7 V/m, material starts to experience a non-linear dependence on the induced electric field in the irradiated material (1.4):

$$P(t) = \varepsilon_0\chi^{(1)}E(t) + \varepsilon_0\chi^{(2)}E^{(2)}(t) + \varepsilon_0\chi^{(3)}E^{(3)}(t) + \cdots \tag{1.4}$$

where ε_0- vacuum dielectric permeability, $\chi^{(1)}$- linear optical sensitivity, $\chi^{(2)}$- second order linear optical sensitivity, $\chi^{(3)}$- third order linear optical sensitivity.

Generally, three types of nonlinear processes can be observed, these are: multiphoton ionization (fig. 2b), tunnelling ionization (fig. 2c) and avalanche ionization (fig. 2d). During the first phenomena with the help of virtual levels an electron is excited from the valance to the conduction band. The probability of such processes occurring is highly dependent on intensity and the band gap energy (1.5):

$$p = \sigma_k I^k \tag{1.5}$$

here k denotes the number of photons, thus $kE_p \geq E_g$ - a necessary condition for multi photon absorption. An observation can be made, that with increase in k a decrease in p occurs. This relation means, that lower-order nonlinearities have a higher probability to happen than higher-order ones.

Another nonlinear effect is tunnelling ionization. Contrary to multiphoton absorption (MPA), tunnelling ionization is a process that is less dependent on the materials band gap energy. It occurs when intense laser radiation distorts the potential barrier of a materials atoms, thus providing a way for the electrons to transition through the potential barrier to the conduction band. A decrease in the potential barrier leads to an increase in the probability of such transitions occurring, thus more and more electrons can transition to the conduction band.

Lastly, a nonlinear process to take note of is avalanche ionization. This process can be separated into two parts: free-carrier absorption and impact ionization. Firstly, an electron that is already in the conduction band linearly absorbs several photons, thus moving into higher energy states of the conduction band. Conservation of both energy and momentum can be performed through the transfer of momentum by absorbing or emitting a phonon or scattering off an impurity when it absorbs a laser photon. For electrons high in the conduction band, the deformation potential scattering time is approximately 1 fs, so frequent collisions make free carrier absorption efficient. After a sufficient number of photons is absorbed by the electron its' energy exceeds the conduction band minimum by more than the band-gap energy of the atom. Colliding with another electron in the valance band ionization can occur. This results in two electrons near the conduction band minimum. Each of these electrons can absorb energy through free-carrier absorption and subsequently additional valence band electrons can impact ionize[16].

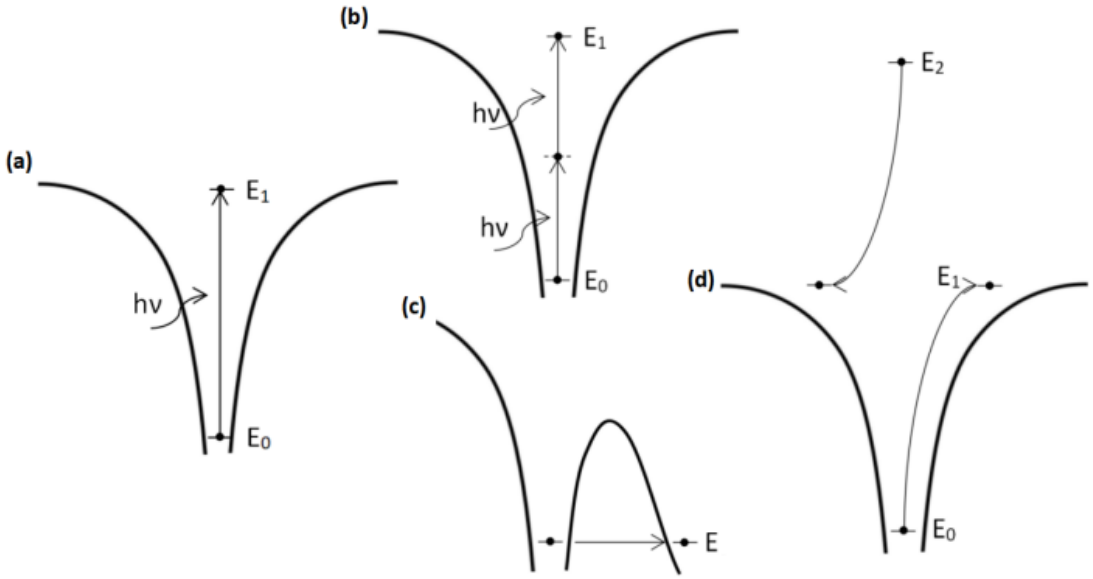

Figure 1. Principle schemes of main nonlinear processes: (a) linear ionization, (b) nonlinear (multiphoton) ionization, (c) tunnelling ionization and (d) avalanche ionization. Image taken from [29].

For a transparent medium, two distinct nonlinear light matter interactions are observed: multiphoton and tunnelling ionization. The dominating regime is defined by the Keldysh parameter (1.5):

$$\gamma = \frac{\omega}{e}\sqrt{\frac{\epsilon_0 cmnE_g}{I}} \tag{1.5}$$

where ω is the frequency of light, e – electron charge, ϵ_0 – dielectric permittivity, c – speed of light, n – refractive index of the material. If $\gamma \ll 1$, the tunnelling ionization is the dominant process, while if $\gamma \gg 1$, the dominant process is multiphoton excitation. In some instances (e.g. fused silica irradiated by 1030 nm laser beam) $\gamma \sim 1$, transitional ionization regime occurs, thus the probability of either multiphoton or tunnelling ionizations happening is equal.

1.2 Additive manufacturing using femtosecond laser

Simply put, almost every manufacturing technique can be divided into five distinct categories, which are: transformative, dividing, joining, subtractive and additive. For simplicities sake, only the latter method will be discussed.

Additive manufacturing (AM) is a method where material is deposited continuously until the structure is completed. Advantages of this technique lies in its ability to create complex geometrical shapes in free space while producing smaller amount of waste in the process. Having said this, the time it takes to create large scale structures using this method is significantly longer than alternative methods, thus usually only limited production runs use this technique. The most widespread adoption of AM was used in casting, however the advancements in 3D printing technologies[17], have widened the capabilities of this technique significantly. Recently the need for smaller, extremely high-resolution structures has emerged. In order to satisfy these needs, techniques using ultra-fast lasers in combination with photosensitive materials have emerged. This combination has enabled fabrication of extreme precision structures, whose feature sizes are in the realm of micrometres. Depending on the application, different light absorption regimes are used. Linear phenomena, such as photolithography and selective laser sintering are widely used for thin film structuring and industrial prototyping respectively. On the other hand, nonlinear effect is mainly utilized for 3D laser lithography. Using this method, a huge variety of elements can be created: mechanically movable structures[18], microfluidic devices[19], [20], biomedical scaffolds[21], micro-optical elements[22].

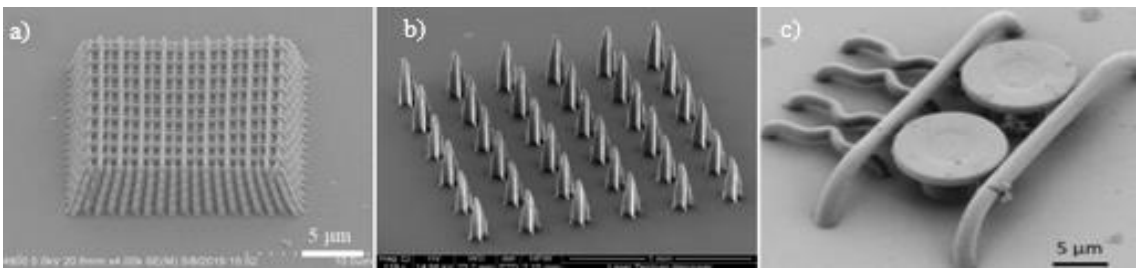

Figure 2. Examples of structures created using 3DLL. a) scaffold, b) microneedle array, c) microdisk resonators. Images are taken from [31], [32] and [33] respectively.

3DLL is a fabrication technique based on multiphoton polymerization (MPP). As mentioned above it is a nonlinear process, thus high intensities are necessary. By applying focusing optics not only is the probability of such transactions to occur increased (section 1.1), but it also enables to define the interaction regime inside a localized volume (voxel). Because of this, true 3D printing can be completed. However, it is important to note, that depending on the focusing optic and intensity of light, laser spot size can change[23]. If adequate conditions are met, features of less than 100 nm can be reached[24], thus achieving sub-wavelength fabrication.

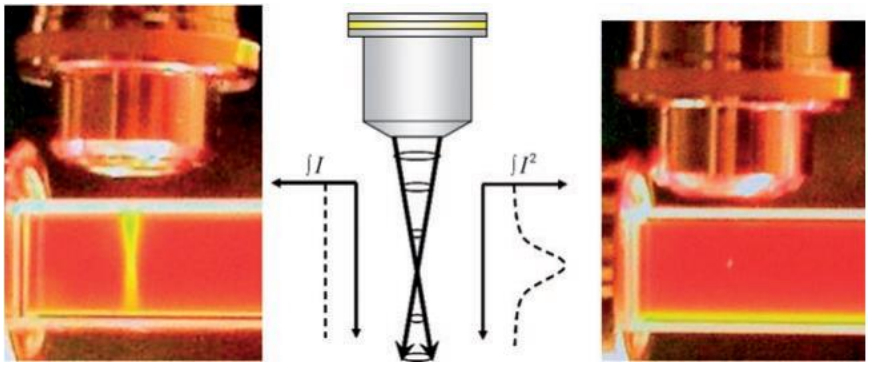

Figure 3. Fluorescence from a solution of rhodamine B caused by single-photon excitation from a UV lamp (left) and by two-photon excitation from a mode-locked Ti:sapphire laser operating at a wavelength of 800 nm (right). The integrated intensity in each transverse section of the beam does not depend upon position for single-photon excitation but is tightly peaked in the focal region for two-photon excitation. Image acquired from [25]

Typical process of 3DLL using MPP is presented in fig. 4. In this case a laser beam is focused inside a prepolymer media, while translational stages and/or galvanometric scanners provide the ability to translate the focal point throughout the sample. Once the beam is focused inside the photosensitive media, dormant photoinitiators (PIs) are excited by MPA. After absorption occurs, the excited PIs form two or more radicals. The formed radicals in turn generate a chain reaction that causes the monomer/oligomers inside the photosensitive polymer create a cross-linked chain. If these bonds are formed tightly enough, the created polymer becomes insoluble in the development solvent, thus surviving the washing step [25].

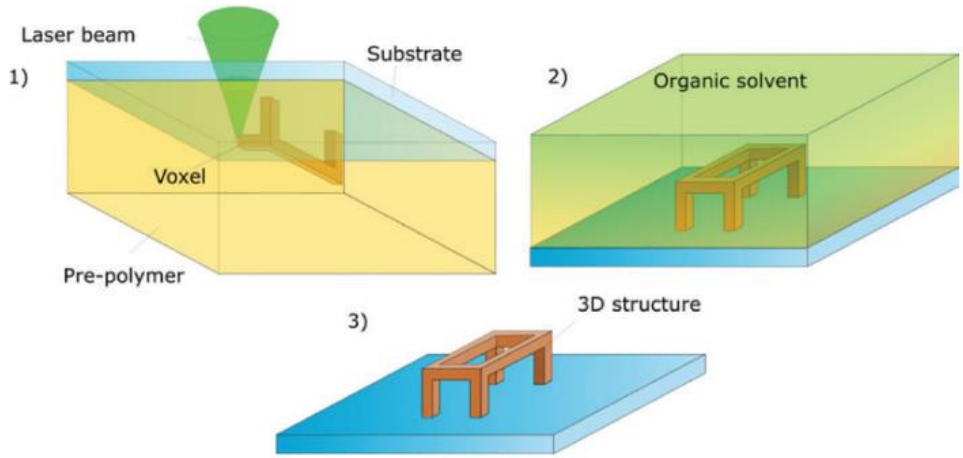

Figure 4. Schematics of multiphoton polymerization-based 3DLL: (1) writing of a structure in prepolymer, (2) development, and (3) final structure. Taken from [30]

It is important to note, that to prevent components from moving during fabrication, the prepolymer resin used is usually a viscous liquid, an amorphous solid or a gel. Each of these options posses their own unique advantages and disadvantages. For example, liquid samples are easier to prepare and process, however undesirable movement of the sample during fabrication can be observed. On the other hand, solid and gel prepolymers require extra steps to be prepared and processed [26]. The upside to these materials is that no motion of the structure is allowed during fabrication, thus more complex structures are possible to be created[25].

1.3 Extending the working distance of an objective

3DLL manufacturing process provides supreme accuracy and resolution for complex structures. As mentioned in section 1.2, voxel sizes are determined by the type of focusing optics used as well as the intensity of the incoming light. In order to achieve sub-wavelength fabrication high NA objectives, need to be used. However, the working distance of such objectives decreases significantly. For example, a 63x/1.4 plan-apochromat objective from Zeiss has a free space working distance of 190 μm, while an 20x0.45 NA objective from Nikon has a working distance of about 6.9-8.2 mm. Techniques such as simultaneous spatiotemporal focusing (SSTF)[27] or dip-in direct laser writing (DIDLW) have been proposed as solutions to this problem. Nevertheless, these methods possess drawbacks as well. For SSTF complex optical changes need to be made, while for DIDLW only a limited number of materials can be processed. It can be also noted, that the resolution of these methods is still lower than by using high NA objectives.

A cheaper and simpler alternative was proposed by K. Obata et. Al. in the form of WOW-2PP[11]. They implemented an additional holder for a common 2PP setup as seen in fig. 5. Using an

additional cover slip in between the objective and the polymer fabrication using a high NA objective can occur over a large area. Mesoscale structure with extremely high resolution can thus be achived.

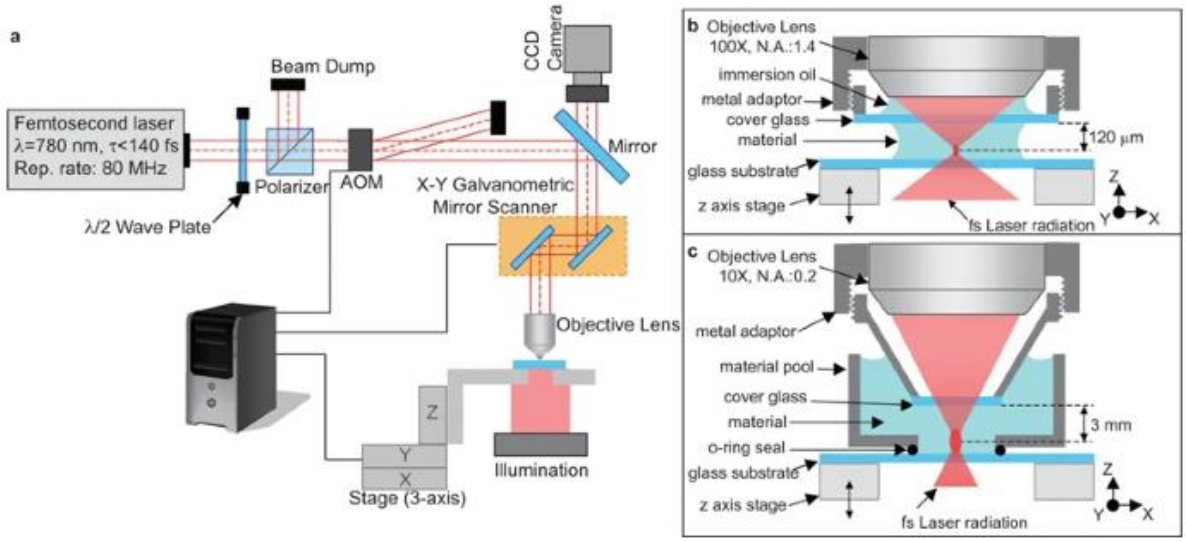

Figure 5. (**a**) Schematic illustration of experimental setup. (**b**) Configuration of WOW-2PP with 100× high-magnification microscope objective. (**c**) Configuration of 10× low-magnification microscope objective. 2PP, two-photon polymerization. Image taken from [11].

2. Experiment process

2.1. Experimental setup

Additive manufacturing was performed with a Menlo fiber oscillator with an operating frequency of 100 MHz and a wavelength of 800 nm thus producing a 100 femtosecond pulses. In order to provide the necessary power for polymerization, the generated impulse is controlled by an acousto-optic modulator (AOM). After passing the AOM, a collimated beam is guided by dichroic mirrors towards a beam expander (BE). Using a BE, a decrease in peak intensity is achieved by the increases of the beam area without significantly affecting the total laser energy, thus ensuring that damage for following optical elements cannot occur. A galvanometric scanner uses two mirrors in order to position the beam inside the field of view of the objective. Beam is then directed towards the objective, where it is then focused onto a single point. The reflected ray from the surface of our sample towards the CMOS camera. A lens is placed if front of the camera in order to focus directly onto its sensor. In this instance the focus variation provides the flexibility of using different objectives without changing the lens itself. In this work an additional holder was used in order to extend the working distance on an objective (fig. 6). Completed schematic view of polymerization setup is presented in fig. 7.

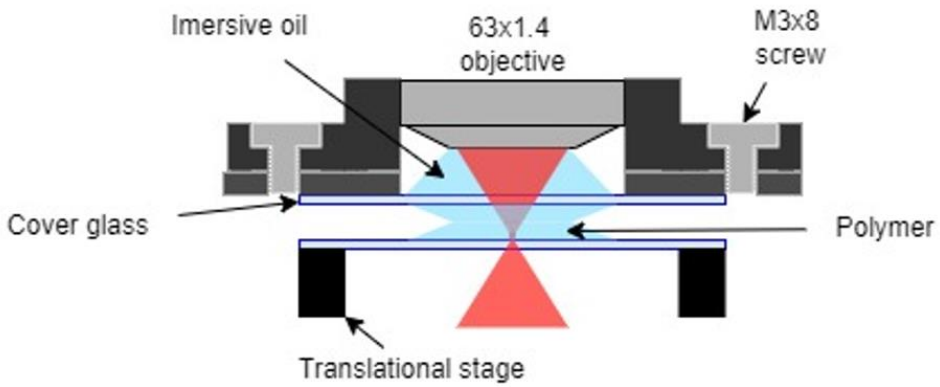

Figure 6. Configuration for polymerization. AOM – acousto-optic modulator, M - dichroic mirrors, BE - beam expander, CMOS - camera used for imaging.

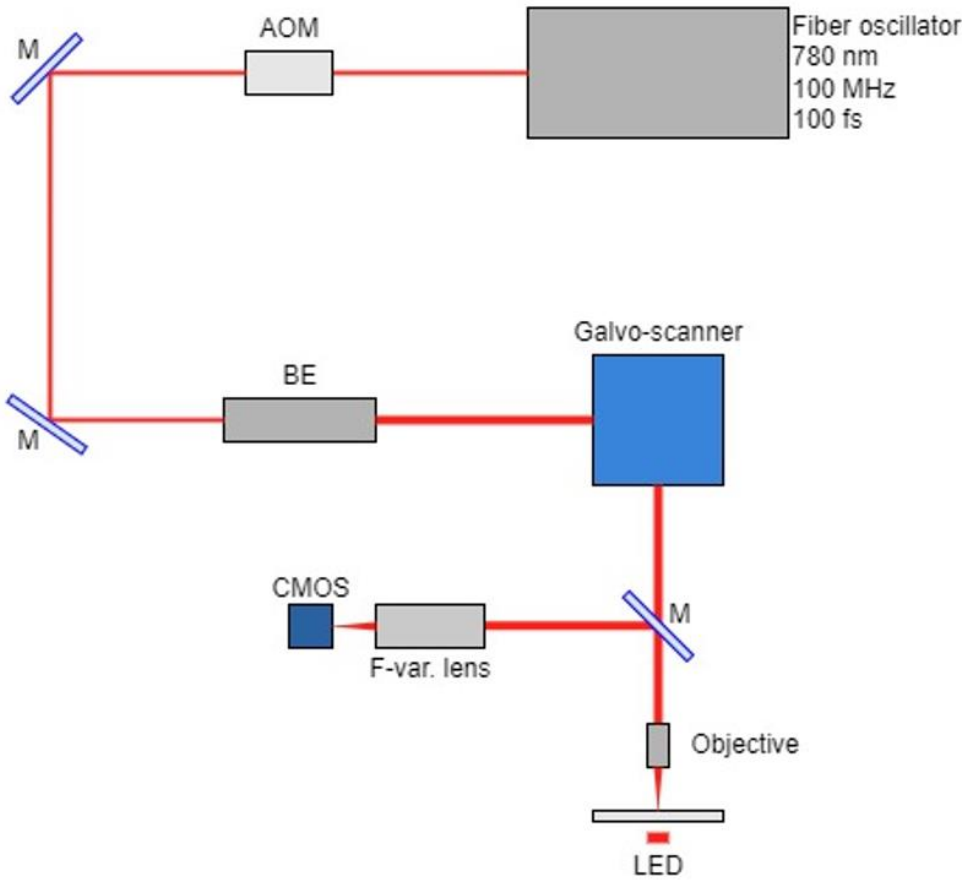

Figure 7. Configuration for polymerization. AOM – acousto-optic modulator, M - dichroic mirrors, BE - beam expander, CMOS - camera used for imaging.

2.2. Manufacturing process

Before manufacturing can begin, 3D objects are required. Creation of such figures was done by using Solidworks 2022 software. Completed structures were then exported in STL format. The exported file is then inspected with 3D view to check for any errors inside the STL. After inspection is complete, the file is then imported to 3DPoli software. In this program the desired object is deconstructed into individual layers. In this program, differently from typical 3D printing applications, an object is defined by the slicing and hatching parameters (fig. 8). Slicing determines the distance between each individual layer, while hatching – the distance between individual lines of a sliced layer. This software also allows the control of manufacturing parameters such as laser power, scanning speed, velocity of translational stage and the position of each axis.

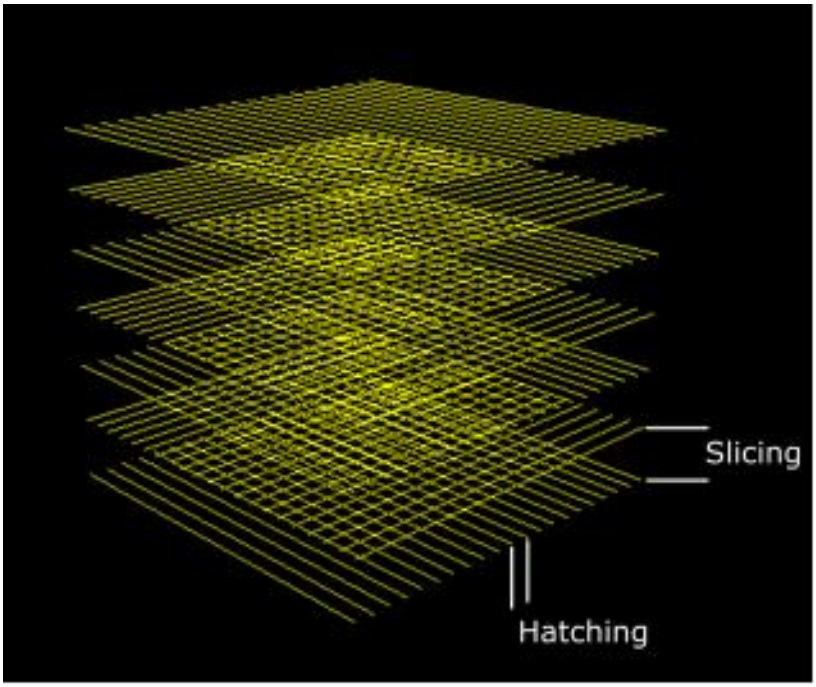

Figure 8. 3DPoli software view of a sliced and hatched cube.

4. Results

4.1 Creation of objective holder

Firstly, creation of a holder capable of extending the working distance of an objective was conducted. Different designs were proposed including off the shelf part assemblies and custom CNC machined parts, however, in order to keep the costs be as minimal as possible it was decided that it will be 3D printed using a Prusa i3 MK3S+. The printed attachment consists of three different parts: two identical parts sides of a cylinder shell as well as a holder onto which cover glass will attach. Because a fused deposition melting (FDM) printer was used, the achievable surface roughness and heights were by an order of magnitude worse than what was needed. In order to combat these errors, solutions were implemented in the design of the attachment. For starters, the cylindrical shell was modelled around the objective. This ensured that the distance to the objective cover glass would be as consistent as it possible. Pins, screws and non-slip materials were used to secure the shell onto the objective. Holder for the cover glass proved to be quite difficult to create. As this attachment is secured to the objective shell via 6 screws, it was essential, that an adequate hole diameter would be present, otherwise inserts could not be threaded in. Another problem arose due to its thickness, which after many iterations a value of 3.5 mm was found to be acceptable. Lastly the cover glass was attached by using optical glue. Completed structure after testing different plastics was made from PLA due to its ease of use and its admissible rigidity (fig. 9).

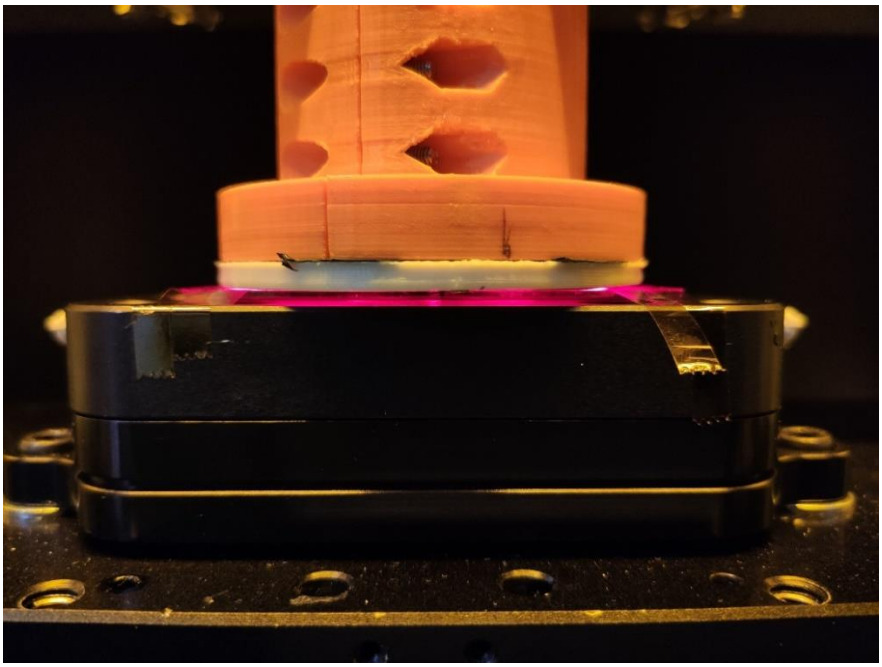

Figure 9. Assembled WOW-2PP holder used in fabrication.

4.2 Extending the working distance of the objective

Before large and complex structures can be created, parameters for manufacturing need to be determined. The values were acquired by completing a resolution test (RT). This procedure creates a 14X10 array of simple structures by varying both laser power and translational stage velocity. Silica glass was selected as the substrate onto which the structures would be made. The glass slide was thus placed onto the sample holder, which uses a small vacuum pump to keep it in place. A drop of polymer ORMOCOMP was then deposited in the centre of the substrate. This guaranteed that when it was squashed by the holder mentioned above, the expanded material would not flow out of the slide area. Before launching the RT, it was determined, that additional fastening of silica glass was necessary. The fixtures were made by placing a couple of kapton strips at both ends of the glass slide. This was done in order to stop glass slides from detaching themselves from the sample holder. Values for the RT were selected as such: velocity of the translational stage was changed from 1000 μm/s to 10000 μm/s with a step value of 1000 μm/s while average laser power was increased from 5 mW to 70 mW with a step value of 5 mW. After the test took place, the sample was then developed by using a constant stream of $C_6H_{12}O$ (izorpopylacetone) drops (fig. 10 (a)). Optimal fabrication parameters were thus selected. Analysis showed that in the range of v_{ts} = 7000 – 10000 μm/s and P_{avg} = 45 – 55 mW fabrication was optimal (fig. 10 (b)).

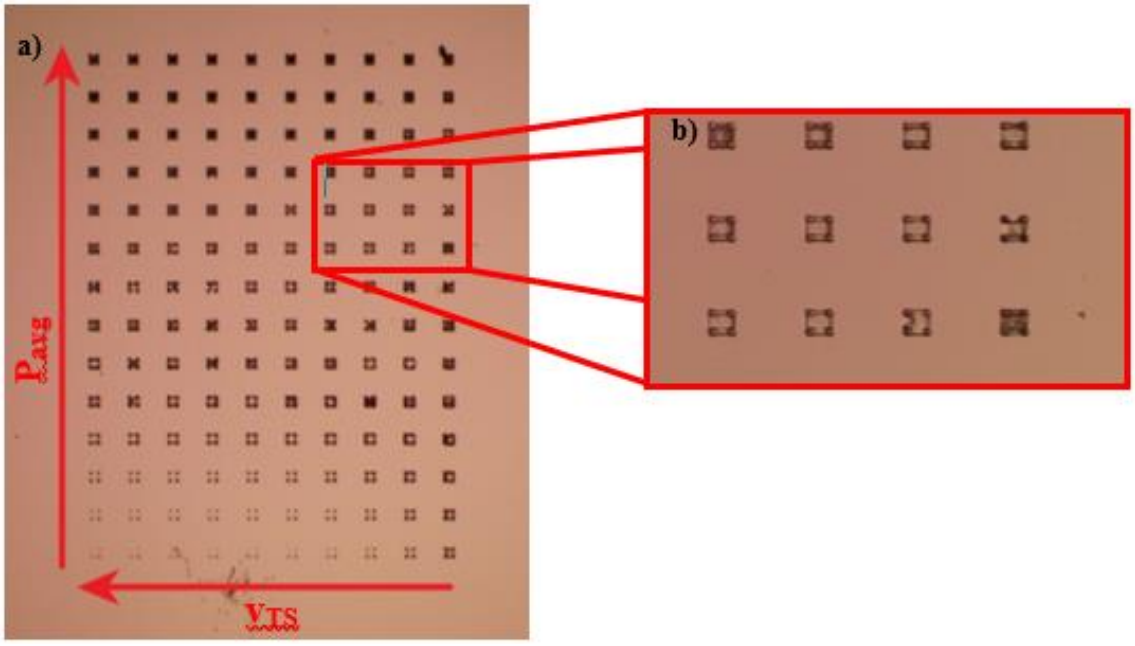

Figure 10. a) Result of the completed RT test after development through a microscope. Arrows direction indicate the increase in value. P_{avg} – average power, v_{TS} – translational stage velocity. b) Acceptable window for fabrication. Here available values are v_{TS} = [7000 – 10000] μm/s while P_{avg} = [45 – 55] mW.

Because the goal of this work is to extend the working distance of a high NA objective, fabrication of high structures was thus done. A solid rod and a double helix spiral were selected as the test figures. These structures were selected as they could provide a general idea on the effects a sample experiences during fabrication. Three samples were decided to be created: a 1 mm high rod and a 500μm as well as a 1 mm hight double helix spiral. Slicing and hatching of 0.2 was set, while the power and translational stage velocity were selected from the fabrication window described above, thus providing values of 55 mW and 10000 μm/s respectively. However, it was clear from the first moments that the aforementioned values are inadequate. Material damage (burning, air bubble formation) as well as the inability for the fabrication layers to properly bond was observed. After several test structures were created the values for laser power were found to be between 15-25 mW while the translational stage velocity of 5000 μm/s was selected. Completed samples are presented in fig. 11.

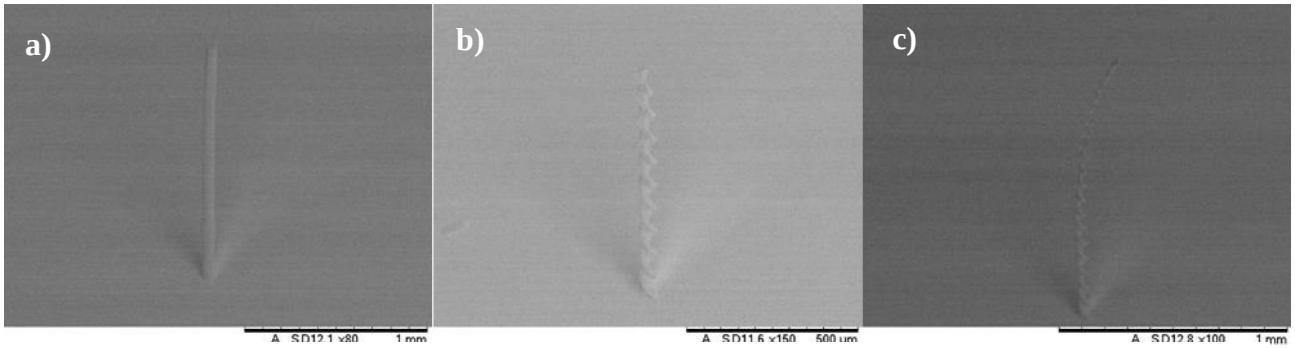

Figure 11. 70 μm diameter 1 mm solid rod as well as 500 μm and 1 mm height double helix spirals.

From these SEM images some unique properties of this configuration and the material can be seen. Firstly, decrease of resolution and mechanical stability was observed. While the simple rod structure did not show any significant changes, this was clearly visible for the double helix spiral, especially when the sample height exceeded 0.5 mm height. These phenomena could be attributed to capillary forces exerted on the sample during fabrication as well as the development process. Another noteworthy property was the flexibility of the structure. Elastic deformations under bending conditions of both double helix spiral (fig. 11 c)) and the solid rod (fig. 12) showed that this material may not be suitable for sub wavelength feature fabrication.

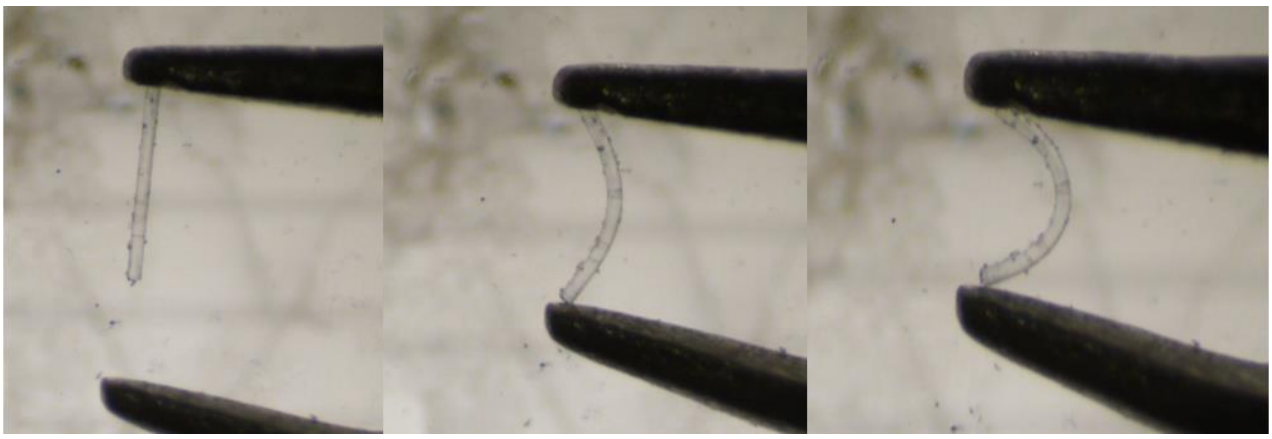

Figure 12. Bending process of a 1 mm solid rod.

While the previous samples showed, the extensions of the working distance of a 64x1.4 NA objective was achieved, even producing result higher than K. Obata et. Al., the working volume was limited to 70x70x1000 μm. In order to demonstrate the capabilities of this configuration, larger structure fabrication was necessary, thus a 500x500x500 μm gyroid cube was selected for this process. Slicing of 0.75 and hatching of 0.2 was selected, while laser power of 25 mW and translational stage velocity of 10000 μm/s was applied. While the aforementioned values proved to be sufficient to successfully complete the structures, issues of layer separation and drop misalignment with the objective optical axis, resulting in partial completion of the sample (fig. 13), were observed. While for the former case solutions such as decreasing translational stage velocity, increasing power or starting the structure inside the silica glass slide could be used, the latter issue required special conditions. Because the additional holder was created by 3D printing while the cover glass is attached via optical glue, surface imperfections and in turn the angle at which it is mounted is hard to evaluate. This issue was solved by mounting the cover plate in such a way, that the cover glass would slightly bend at the objective centre.

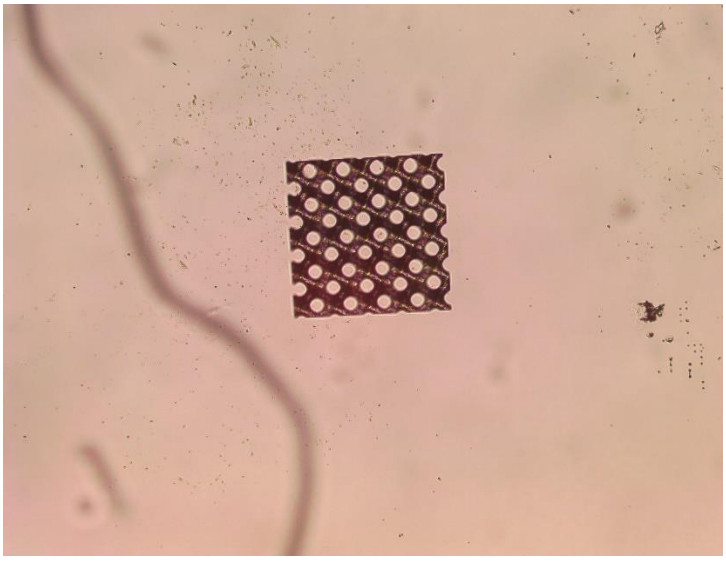

Figure 13. Microscope view of a partially completed 500x500x500 μm gyroid structure. A height between 200-250 μm was estimated by adjusting the focus of the objective.

Fixing these issues allowed for the creation of a 500x500x500 μm structure (fig. 14 a)). Achieving this height proved that by using this configuration working distance of the objective can be easily increased. In order to improve the result more fabrication of a mesoscale 1x1x1 mm size gyroid was performed. Parameters for hatching, slicing, beam power and translational stage velocity remained unchanged. Develped sample SEM images are presented in fig. 14 b).

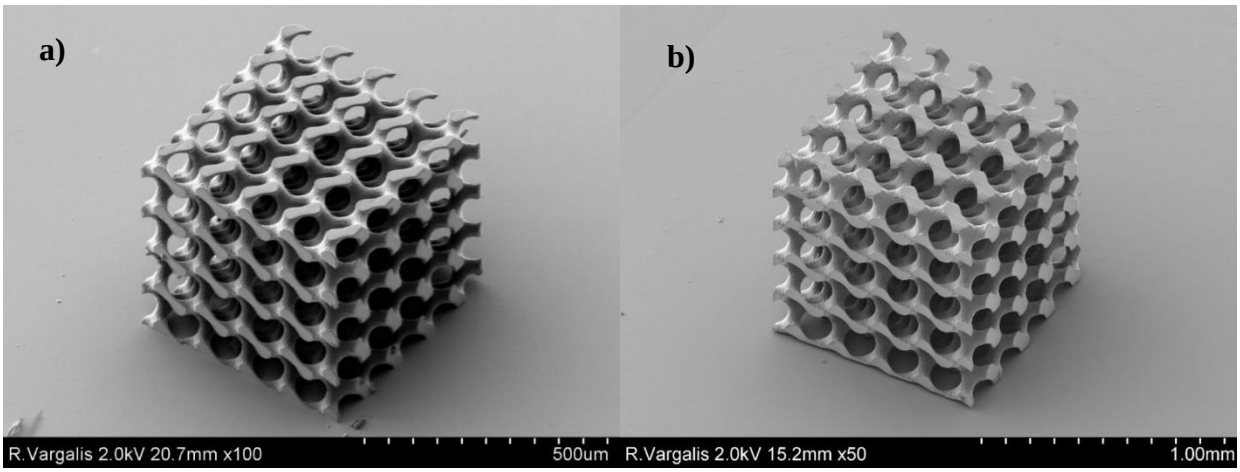

Figure 14. SEM image of a) 0.5x0.5x0.5 mm, b) 1x1x1 mm gyroid cube.

Because a high numerical aperture objective was used during fabrication, small voxel sizes and in turn high resolutions are possible to be achieved. Having said this, these gyroid structures do not require such high resolutions, thus by using lower NA objectives, the fabrication time could be drastically decreased. On the other hand, high surface quality is easily achievable with this configuration as seen in fig. 15.

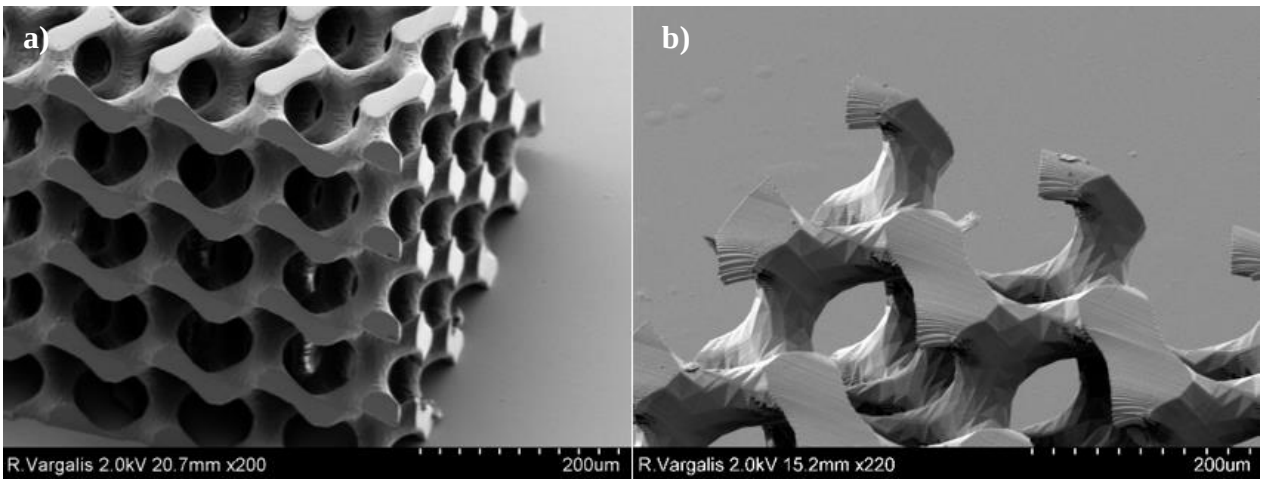

Figure 15. Close up SEM image of 0.5x0.5x0.5 mm (left) and 1x1x1 mm (right) gyroid cube. It can be seen that the surface quality of the completed structure is limited by the initial resolution of the sample .STL file.

4.3 Creation of auxetic structures

As previously shown objects, exceeding the working distance of the objective have been created. In order to take full advantage of high NA objectives, small feature size objects are necessary. Having said this, observation of the material elasticity showed, that sub wavelength fabrication may be hard to achieve. Taking these things into account, a decision has been made to produce mechanical re-entrant auxetic materials.

Using Solidworks 2022 software the desired structures were created with different lattice counts (fig. 16). Design of these figures was modelled after the work of[28]. Because the features of these samples were significantly smaller than in section 4.2, new fabrication parameter were necessary. The need for this change was observed, when the completed structure would collapse on itself during development or would fail to fully fabricate.

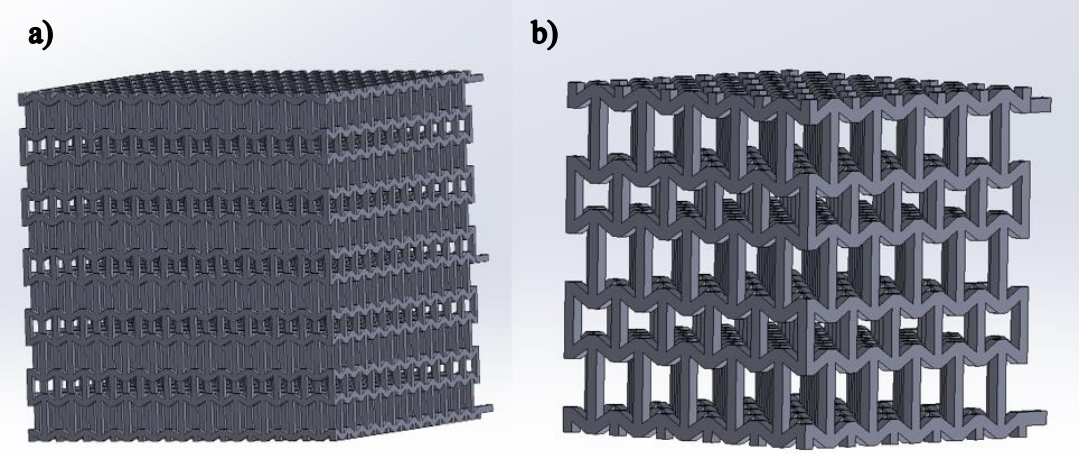

Figure 16. Auxetic structures models with varying lattice counts a) 762 b) 75.

Having these findings in mind, fabrication of the re-entrant structures then was completed. A 500 and a 300 µm figures, with respective lattice counts from fig. 14, were made. In order to limit the negative effects that occur during their manufacturing process, the structures were created with a translational stage velocity of 3500 µm/s and hatching/slicing of 0.5. Completed samples are presented in fig. 17.

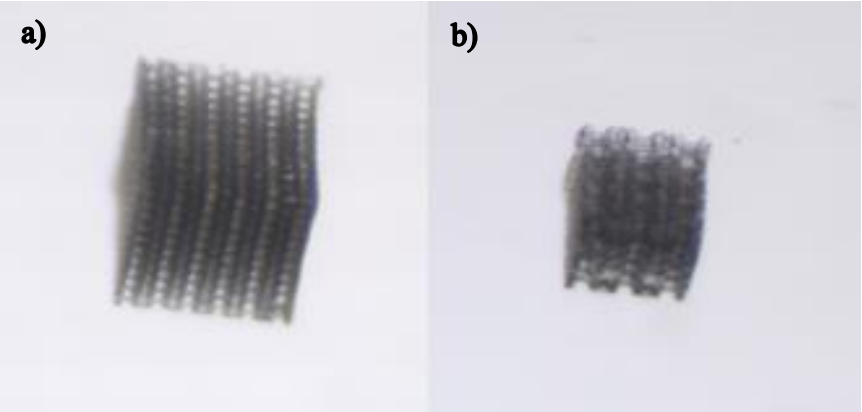

Figure 17. Completed 500 µm (a) and 300 µm (b) samples.

Testing of the auxetic structure behaviour was conducted by using pliers and is presented in fig 18. From these images we can see that the structures did not operate as true re-entrant material. This could be cause by the aforementioned elasticity of the finished sample, thus requiring to consider other configurations, or due to incorrect direction of the applied pressure. It can be also observed, that the 300 µm sample could deform significantly more as compared to the 500 µm structure. This is likely caused by smaller latices in the latter sample, thus increasing the fill factor and the distance the lattices can deform.

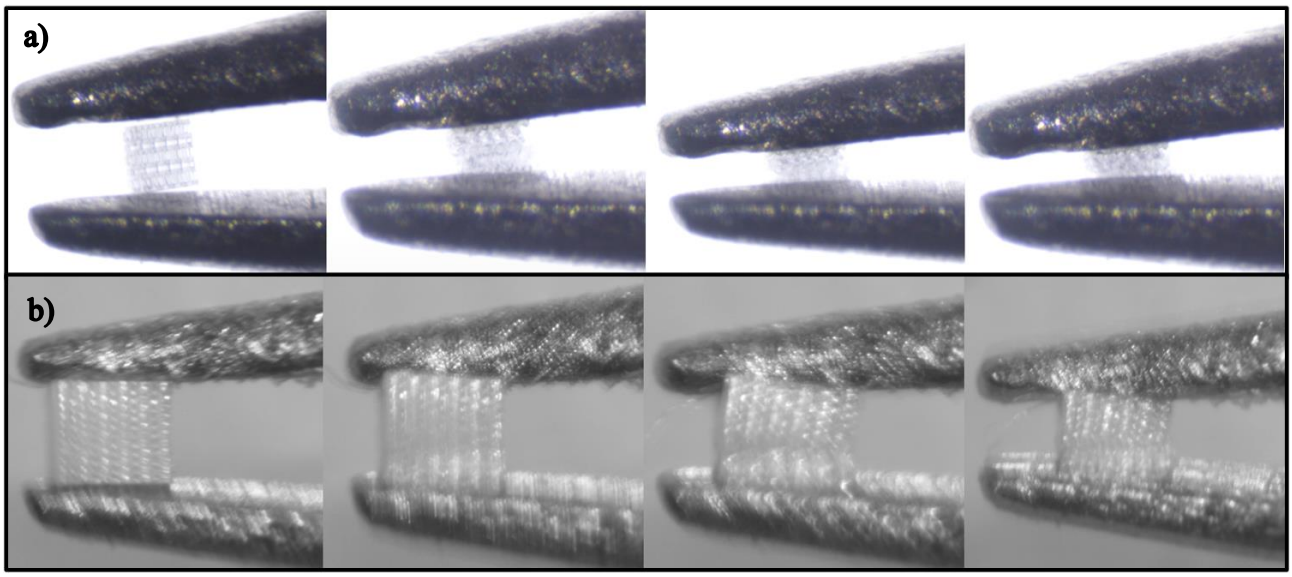

Figure 18. Deformation testing of 300 µm (a) and 500 µm (b) re-entrant structures.

Measuring the feature size of these constructions was done by using Heliotis HeliInspect H8 white-light interferometer. Acquired measurements were then exported as .TIF and .SUR files. Importing former files to ImageJ software, feature sizes were evaluated with reference measurement, while the latter files were selected to show the topographical view of the finished structures (fig. 19).

From these results we can see that for the 300 µm lattice the feature size is about 10 µm, while for the larger one, features of ~6 µm were achieved.

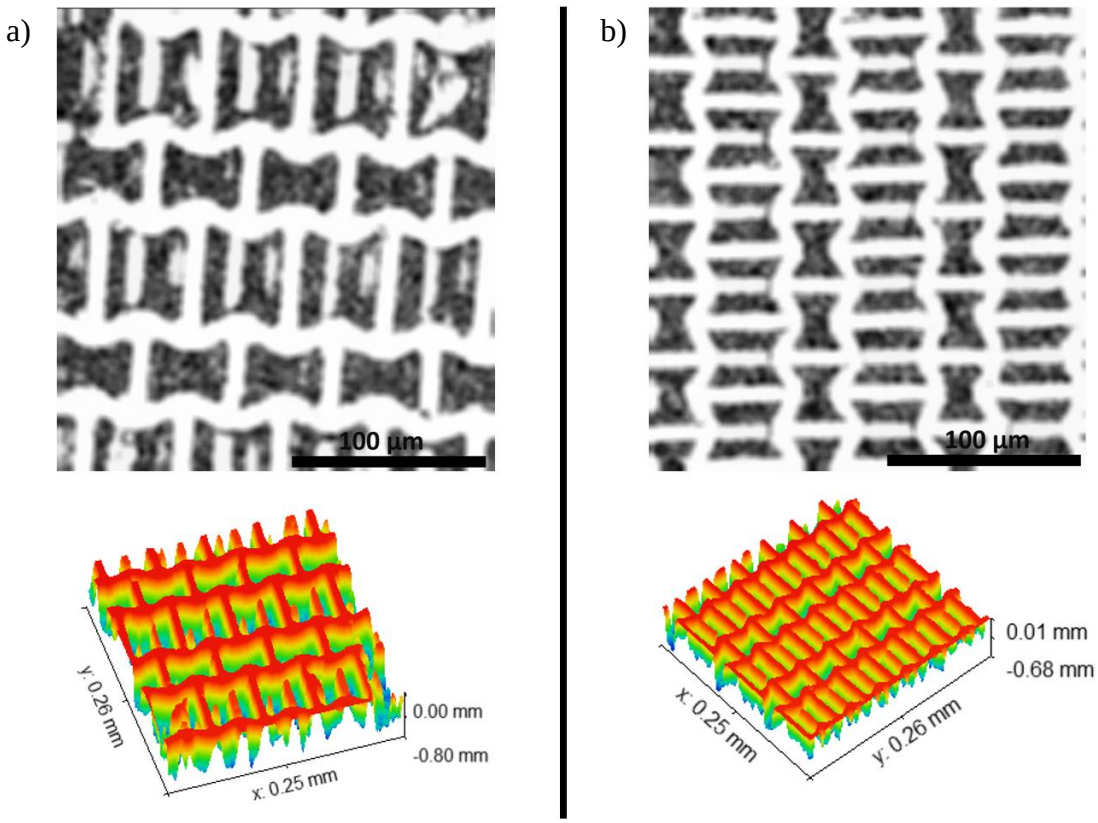

Figure 19. HeliInspect view of 300 µm (a) and 500 µm (b) of auxetic structures.

5. Discussion

During this course work a cheap and easy method for extending the working distance of an objective was demonstrated. An initial working distance of an 63x1.4 NA objective was increased from 190 µm to 1 mm. While this change shows an increase of more than 5 times as compared to initial conditions, however, typically the operating working distance is much lower. Because the objective cannot be immersed inside the polymer, fabrication is done through a thin (≥100 µm) borosilicate glass slide, thus producing structures less than 90 µm in height. Taking these conditions into account, it can be argued that an extension of more than 10 times the initial working distance has been achieved during this work, while by applying 3DLL principles complex geometrical shapes were created.

Manufacturing of such structures shows that WOW-2PP has yet unexplored possibilities. Creation of millimetre sized objects with micrometre scale features could be implemented in various fields. As the provided method used an already existing polymerization setup, purposely built systems

could thus produce even better results. Having said this, the time it take to complete such structure may lead to this technique being commercially unviable.

6. Conclusion

1. A cheap and easy to produce device was created for extending the working distance of an objective for present polymerization setup.
2. The working distance of a 63x1.4 objective was increased more than 5 times, however, if operating condition are to be considered, increase of more than 10 times can be argued.
3. Fabricated auxetic re-entrant structures with resolution of couple of μm was reached, however due to innate polymer properties smaller feature sizes were difficult to achive.

Abstract

Ultrafast lasers have become a staple in various fields. Implementation of these devices has provided a way to use them contact-free tool, which is capable of extreme precision for both macro and micro machining. An interesting field of study for the latter area is AM, or more precisely, 3DLL. This technology allows to create complex geometrical 3D structures with feature sizes in nm range. However, resolution and the structure size of such systems is limited by the NA of the objective. To extend the working distance of high NA objectives, a solution called WOW-2PP[21] has been proposed.

The goal of this work was to provide a method for creating large-scale structures with micrometre sized features. This was completed by creating a custom holder for the 63x1.4NA objective. High viscosity polymer (Ormocers Ormocmp) was used during the fabrication process. Finished structures were inspected by using optical microscope, white light interferometer and a scanning electron microscope.

During this work various observations were made. Firstly, structures possessing small features required lower stage velocities (≤5000 μm/s), otherwise the desired geometries would fail to fabricate. It was also noted, that because the finished polymer sample had extremely high elasticity, high resolutions were difficult to achieve. Having said this, the latter property showed to be quite usefull for the fabrication of re-entrant auxetic strucutres.

Santrauka

Ultragreiti lazeriai tapo nepamainomi įvairuose srityse. Šių įrenginių įdiegimas sudarė galimybes juos naudoti kaip bekontakčius įrankius, galinčius pasiekti itin tikslaus makro ir mikro apdirbimo. Įdomus pastarosios srities pritaikymas yra AM,arba tikslaiu 3DLL. Ši technologija leidžia sukurti sudėtingas geometrines 3D struktūras, kurių dalis gali siekti nm eilę. Vis dėlto, darinių raiška ir dydis pasiekiamas šiomis sistemomis yra apriboti objectyvo NA. Siekant padidinti darbinį atstumą aukštos NA objectyvų, metodas, vadinamas WOW-2PP[21], buvo pasiūlytas.

Šio darbo tikslas buvo sukurti metodą skirtą didelių struktūrų pasižyminčių mikrometrų dydžio dalimis fabrikavimui. Šitai buvo pasiekta sukuriant prototipinį laikiklį skirtą 63x1,4 NA objektyvui. Lakus polimeras (Ormocer ORMOCOMP) buvo naudotas fabrikacijos metu. Baigtos struktūros buvo apžiūrėtos naudojant optinį mikroskopą, baltos šviesos interferometra ir skenuojantį elektronų mikroskopą.

Darbo metu buvo padaryti įvairūs pastebėjimai. Pirmiausia, struktūroms, turinčioms mažas dalis, fabrikacijos metu buvo reikalingi mažesni judamųjų stalų greičiai (≤5000 μm/s), kitu atveju norimos geometrijos nebūtų gautos. Taip pat buvo pamatyta, jog baigti polimeriniai junginiai pasižymėjo ypač dideliu elastingumu, kuris trukdė pasiekti aukštą bandinių raišką. Vis dėlto, pastaroji medžiagos savybė buvo naudinga fabrikuojant meta medžiagų struktūras.

References

[1] T. H. Maiman, “Stimulated Optical Radiation in Ruby,” *Nature 1960 187:4736*, vol. 187, no. 4736, pp. 493–494, 1960, doi: 10.1038/187493a0.

[2] M. Horowitz, C. R. Menyuk, T. F. Carruthers, and I. N. Duling, “Theoretical and experimental study of harmonically modelocked fiber lasers for optical communication systems,” *Journal of Lightwave Technology*, vol. 18, no. 11, pp. 1565–1574, Nov. 2000, doi: 10.1109/50.896218.

[3] C. Herbert *et al.*, “Discrete mode lasers for communication applications,” *IET Optoelectronics*, vol. 3, no. 1, pp. 1–17, 2009, doi: 10.1049/IET-OPT:20080028.

[4] J. D. Majumdar, I. Manna “Laser-Assisted Fabrication of Materials”, 2012

[5] M. Domke, S. Wick, M. Laible, S. Rapp, H. P. Huber, and R. Sroka, “Ultrafast dynamics of hard tissue ablation using femtosecond-lasers,” *J Biophotonics*, vol. 11, no. 10, Oct. 2018, doi: 10.1002/JBIO.201700373.

[6] C. v. Gabel, “Femtosecond lasers in biology: nanoscale surgery with ultrafast optics,” *http://dx.doi.org/10.1080/00107510802628263*, vol. 49, no. 6, pp. 391–411, Nov. 2009, doi: 10.1080/00107510802628263.

[7] S. H. Chung and E. Mazur, “Surgical applications of femtosecond lasers,” *J Biophotonics*, vol. 2, no. 10, pp. 557–572, Oct. 2009, doi: 10.1002/JBIO.200910053.

[8] K. Isobe, W. Watanabe, and K. Itoh, “Ultrafast Laser Surgery,” *Functional Imaging by Controlled Nonlinear Optical Phenomena*, pp. 327–341, Sep. 2013, doi: 10.1002/9781118751879.CH6.

[9] S. M. Metev, V. P. Veiko “Laser-Assisted Microtechnology.”, 1998.

[10] X. Zhou, Y. Hou, and J. Lin, “A review on the processing accuracy of two-photon polymerization,” *AIP Adv*, vol. 5, p. 30701, 2015, doi: 10.1063/1.4916886.

[11] K. Obata, A. El-Tamer, L. Koch, U. Hinze, and B. N. Chichkov, “High-aspect 3D two-photon polymerization structuring with widened objective working range (WOW-2PP),” *Light: Science & Applications 2013 2:12*, vol. 2, no. 12, pp. e116–e116, Dec. 2013, doi: 10.1038/lsa.2013.72.

[12] “Absorption, explained by RP Photonics Encyclopedia; light, processes, linear and nonlinear, parasitic, thermal effects, quantum noise.” https://www.rp-photonics.com/absorption.html (accessed Jun. 28, 2022).

[13] J. N. Gonsalves and W. W. Duley, “Cutting thin metal sheets with the cw CO2 laser,” *J Appl Phys*, vol. 43, no. 11, p. 4684, Nov. 2003, doi: 10.1063/1.1660989.

[14] H. K. Tönshoff, L. Overmeyer, A. Ostendorf, and H. Hesener, “NEW MACHINING CONCEPT FOR MANUFACTURING MICROSTRUCTURES WITH EXCIMER LASERS,” *http://dx.doi.org/10.1080/10940349708945642*, vol. 1, no. 1, pp. 153–162, 2007, doi: 10.1080/10940349708945642.

[15] “OrmoComp® – Microresist.” https://www.microresist.de/en/produkt/ormocomp/ (accessed Jun. 28, 2022).

[16] C. B. Schaffer, A. Brodeur, and E. Mazur, “Laser-induced breakdown and damage in bulk transparent materials induced by tightly focused femtosecond laser pulses,” *Meas Sci Technol*, vol. 12, no. 11, p. 1784, Oct. 2001, doi: 10.1088/0957-0233/12/11/305.

[17] D. Srinivasan *et al.*, “3D Printing Manufacturing Techniques, Materials, and Applications: An Overview,” *Advances in Materials Science and Engineering*, vol. 2021, 2021, doi: 10.1155/2021/5756563.

[18] L. Jonušauskas, T. Baravykas, D. Andrijec, T. Gadišauskas, and V. Purlys, “Stitchless support-free 3D printing of free-form micromechanical structures with feature size on-demand,” *Scientific Reports 2019 9:1*, vol. 9, no. 1, pp. 1–12, Nov. 2019, doi: 10.1038/s41598-019-54024-1.

[19] J. Wu, M. Dong, C. Rigatto, Y. Liu, and F. Lin, “Lab-on-chip technology for chronic disease diagnosis,” *npj Digital Medicine 2018 1:1*, vol. 1, no. 1, pp. 1–11, Apr. 2018, doi: 10.1038/s41746-017-0014-0.

[20] J. P. Conde *et al.*, “Lab-on-chip systems for integrated bioanalyses,” *Essays Biochem*, vol. 60, no. 1, pp. 121–131, Jun. 2016, doi: 10.1042/EBC20150013.

[21] S. Schlie *et al.*, “Three-dimensional cell growth on structures fabricated from ORMOCER® by two-photon polymerization technique,” *J Biomater Appl*, vol. 22, no. 3, pp. 275–287, Nov. 2007, doi: 10.1177/0885328207077590.

[22] E. Stankevičiusa, M. Malinauskas, and G. Račiukaitis, “Fabrication of scaffolds and micro-lenses array in a negative photopolymer SZ2080 by multi-photon polymerization and four-femtosecond-beam interference,” *Phys Procedia*, vol. 12, no. PART 2, pp. 82–88, 2011, doi: 10.1016/J.PHPRO.2011.03.109.

[23] L. Jonusauskas, “Linas JONUŠAUSKAS 3D Laser Lithography of Meso-Scale Structures: Towards Applications”, doi: 10.15388/vu.thesis.145.

[24] J. M. Hales *et al.*, “65 nm feature sizes using visible wavelength 3-D multiphoton lithography,” *Optics Express, Vol. 15, Issue 6, pp. 3426-3436*, vol. 15, no. 6, pp. 3426–3436, Mar. 2007, doi: 10.1364/OE.15.003426.

[25] C. N. LaFratta, J. T. Fourkas, T. Baldacchini, and R. A. Farrer, “Multiphoton fabrication,” *Angewandte Chemie - International Edition*, vol. 46, no. 33, pp. 6238–6258, 2007, doi: 10.1002/ANIE.200603995.

[26] M. Farsari, M. Vamvakaki, and B. N. Chichkov, “Multiphoton polymerization of hybrid materials,” *Journal of Optics*, vol. 12, no. 12, 2010, doi: 10.1088/2040-8978/12/12/124001.

[27] W. Chu *et al.*, “Centimeter-Height 3D Printing with Femtosecond Laser Two-Photon Polymerization,” *Adv Mater Technol*, vol. 3, no. 5, May 2018, doi: 10.1002/ADMT.201700396.

[28] S. Maran, I. G. Masters, and G. J. Gibbons, “Additive Manufacture of 3D Auxetic Structures by Laser Powder Bed Fusion—Design Influence on Manufacturing Accuracy and Mechanical Properties,” *Applied Sciences 2020, Vol. 10, Page 7738*, vol. 10, no. 21, p. 7738, Nov. 2020, doi: 10.3390/APP10217738.

[29] L. Jonušauskas, R. Martínez Vázquez, F. Bragheri, and P. Paiè, “3D Manufacturing of Glass Microstructures Using Femtosecond Laser,” *Micromachines 2021, Vol. 12, Page 499*, vol. 12, no. 5, p. 499, Apr. 2021, doi: 10.3390/MI12050499.

[30] L. Jonušauskas, D. Mackevičiute, G. Kontenis, and V. Purlys, “Femtosecond lasers: The ultimate tool for high-precision 3D manufacturing,” *Advanced Optical Technologies*, vol. 8, no. 3–4, pp. 241–251, Jun. 2019, doi: 10.1515/AOT-2019-0012.

[31] W. Gao *et al.*, “Ionic Carbazole-Based Water-Soluble Two-Photon Photoinitiator and the Fabrication of Biocompatible 3D Hydrogel Scaffold,” *ACS Appl Mater Interfaces*, vol. 13, no. 24, pp. 27796–27805, Jun. 2021, doi: 10.1021/ACSAMI.1C02227/SUPPL_FILE/AM1C02227_SI_001.PDF.

[32] S. D. Gittard, A. Nguyen, K. Obata, A. Koroleva, R. J. Narayan, and B. N. Chichkov, “Fabrication of microscale medical devices by two-photon polymerization with multiple foci via a spatial light modulator,” *Biomed Opt Express*, vol. 2, no. 11, p. 3167, Nov. 2011, doi: 10.1364/BOE.2.003167.

[33] A. J. G. Otuka, N. B. Tomazio, K. T. Paula, and C. R. Mendonça, “Two-Photon Polymerization: Functionalized Microstructures, Micro-Resonators, and Bio-Scaffolds,” *Polymers 2021, Vol. 13, Page 1994*, vol. 13, no. 12, p. 1994, Jun. 2021, doi: 10.3390/POLYM13121994.